Direct links between hygroscopicity and mixing state of ambient aerosols: Estimating particle hygroscopicity from their single particle mass spectra

Xinning Wang[1], Xingnan Ye[1], Jianmin Chen[1], Xiaofei Wang*[1,2], Xin Yang*[1,2,3],
Tzung-May Fu[3], Lei Zhu[3], Chongxuan Liu[3]

[1] Shanghai Key Laboratory of Atmospheric Particle Pollution and Prevention, Department of Environmental Science and Engineering, Fudan University, Shanghai, China

[2] Shanghai Institute of Pollution Control and Ecological Security, Shanghai, China

[3] School of Environmental Science and Engineering, Southern University of Science and Technology, Shenzhen, China

Atmospheric Chemistry and Physics

April 2nd, 2020

*To whom correspondence should be addressed.

Correspondence to:

Xiaofei Wang: Email: xiaofeiwang@fudan.edu.cn Tel: +86-21-31242526

Xin Yang: Email: yangxin@fudan.edu.cn Tel: +86-21-31245272

ABSTRACT

Hygroscopicity plays crucial roles in determining aerosol optical properties and aging processes in the atmosphere. We investigated submicron aerosol hygroscopicity and composition by connecting an aerosol time-of-flight mass spectrometer (ATOFMS) in series to a hygroscopic tandem differential mobility analyzer (HTDMA), to characterize hygroscopicity and composition of ambient aerosols in Shanghai, China. The HTDMA-ATOFMS data suggested that particle types, including biomass burning, EC, Dust/Ash, organics particles, cooking particles and sea salt, were shown to have distinct hygroscopicity distributions. Peak intensities in particle spectra were found nonlinearly correlated with hygroscopicity and the correlations were variant with particle types. Based on the measured hygroscopicity-composition relations, we developed a statistical method to estimate ambient particle hygroscopicity just from their mass spectra. The method was applied to another ambient ATOFMS dataset sampled during September 12nd to 28th, 2012 in Shanghai. The estimated hygroscopicity suggested that ambient particles were present in three apparent hygroscopicity modes, whose growth factors peaked at 1.05, 1.42 and 1.60 (85% RH), respectively. The estimated GF were divided into four bins as <1.1, 1.1-1.3, 1.3-1.5 and >1.5 to represent the nearly-hydrophobic (NH), less-hygroscopic (LH), more-hygroscopic (MH) and sea salt (SS) mode. Number contributions of particle types to hygroscopicity modes showed consistent results with the HTDAM-ATOFMS experiment. Based on the combined information on particle composition, hygroscopicity, airmass back trajectories and ambient pollutants concentrations, we inferred that the NH, LH, MH, SS modes were characterized by POA/EC, SOA, SIA and salts compositions, respectively. The proposed method would provide additional information to the study of particle mixing states, source identification and visibility degradation.

1. INTRODUCTION

Atmospheric particles have critical impacts on climate and the environment. They affect climate by directly interacting with sunlight and changing the energy balance of earth's atmosphere (Facchini et al., 1999;Lohmann and Feichter, 2005). Aerosol particles also act as cloud condensation nuclei or ice nuclei and impact cloud formation (Lohmann and Feichter, 2005). Aerosol particles provide surfaces for heterogeneous reactions to occur and act as the sink for many atmospheric reactions (Gard et al., 1998;Qiu and Zhang, 2013), which are of significance to air quality, visibility and human health. The climate-relevant and other properties of aerosols are largely determined by their hygroscopicity. In atmospheric conditions the hygroscopic growth transform particles into micro droplets and their optical effects are altered importantly (Cheng et al., 2008;Qu et al., 2015), which further impacts particle aging processes and visibility degradation (Qu et al., 2015;Liu et al., 2012;Qiu and Zhang, 2013;Chen et al., 2012).

Atmospheric particles are a mixture of a complicated variety of chemical compounds. The bulk chemical composition of particulate matter (PM) usually refers to its dry composition. However, in ambient conditions the particulate water is also an important constitution of PM which has not been accounted for in conventional gravitational analysis. The mass of particulate water may be much larger than the total mass of dried PM at elevated RHs (Swietlicki et al., 2008). The factors that affect water contents in particles include the particle hygroscopicity, the particle size distributions and ambient RH. The hygroscopicity parameter determines the particle's ability to growth in their sizes in humidity environment, which is directly relates to particle composition and size. To accurately predict particulate water content, a detailed knowledge on particle hygroscopicity and composition is needed (Gysel et al., 2007;Sjogren et al., 2008;Laborde et al., 2013;Healy et al., 2014).

Aerosol hygroscopicity can be quantitatively measured by techniques such as the Hygroscopic Tandem Differential Mobility Analyzer (HTDMA) (Swietlicki et al., 2008). Previous studies measured aerosol hygroscopicity and chemical composition simultaneously by deploying HTDMA and chemical composition measurements in parallel (Gysel et al., 2007;Sjogren et al., 2008;Laborde et al., 2013). The measured hygroscopicity was compared with the reconstructed values using the mixing rules of variant compositions (Gysel et al., 2007). The hygroscopicity reconstructed in this way is representing the averaged hygroscopicity of ensembled particles and therefore could not reflect the mixing states of particles (Healy et al., 2014). However, the HTDMA measurements suggested that several hygroscopicity modes exist simultaneously, which evidenced the external mixing state of atmospheric particles. HTDMA hygroscopicity modes were generally fell into four categories: nearly hydrophobic (NH), less-hygroscopic (LH), more-hygroscopic (MH), and sea-salt mode, with their center GFs (90% RH) lie in 1.0-1.11, 1.11-1.33, >1.33 and >1.8 ranges, respectively (Swietlicki et al., 2008). To investigate the chemical nature of these hygroscopicity modes, it is better to connect HTDMA and composition measurement techniques in tandem, since more direct connection between hygroscopicity and composition could be established in this way (Buzorius et al., 2002;Zelenyuk et al., 2008;Herich et al., 2008;Laborde et al., 2013). For composition measurement techniques, single particle mass spectrometers are preferred since they are sensitive to analyze particles of low concentrations in the HTDMA outflow (Herich et al., 2008;Herich et al., 2009), and that the particle mixing state information is preserved during analysis (Healy et al., 2014).

Only a few studies have reported simultaneous characterization of hygroscopicity and composition using the tandem method (Herich et al., 2008;Herich et al., 2009;Buzorius et al., 2002;Zelenyuk et al., 2008). Zelenyuk et al. connected a single particle mass spectrometer SPLAT with HTDMA to demonstrate the capability of this system to derive quantitative information on aerosol hygroscopicity, composition, and effective density (Zelenyuk et al., 2008). Herich et al. firstly applied the tandem HTDMA-ATOFMS system to characterize particle composition of different hygroscopicity (Herich et al., 2008;Herich et al., 2009). A large portion of the less hygroscopic modes were found to be contributed by organics and combustion species both in the urban and remote site, while the sulfates and nitrates were present in almost all particles independent of hygroscopicity. Similar findings were also observed in our preliminary characterization using HTDMA-ATOFMS in Shanghai city (Wang et al., 2014), except higher nitrate and sulfate intensities were found in hygroscopic particles in our study. However, the preliminary dataset was not sufficiently large since only a few GF were characterized in that study (GF 1.05-1.1, 1.3, 1.4 and 1.5 at 85% RH). The primary objective of the present study is to establish more complete connections between hygroscopicity and single particle signatures, which could be further utilized to predict hygroscopicity of ambient particles. We conducted a comprehensive HTDMA-ATOFMS experiment with the particle GF varied in a more complete range (0.9~1.7, 85% RH), which accounted for the main number fraction of atmospheric particles in urban atmosphere (Liu et al., 2014;Liu et al., 2011;Ye et al., 2013) . Based on the HTDMA-ATOFMS data, we further developed and tested a method to estimate the hygroscopicity of ambient particles analyzed by ATOFMS.

2. EXPERIMENTAL SECTION

2.1. HTDMA

The custom-built HTDMA (Ye et al., 2009) consists of two DMAs and a humidifier connected in series (Figure 1). Aerosol was dried before entering HTDMA (RH ~10%) by a diffusional silica gel tube. The dried aerosol reached charge equilibrium in a Kr-85 neutralizer. The DMA1 (Model 3081, TSI Inc.) selected particles by electrical mobility size as D_{dry}. The monodisperse particles from DMA1 grew in a Nafion humidifier (RH=85%). The sizes of humidified particles D_{RH} was determined by the second DMA connected by a CPC to measure their concentrations. The sheath flow rate in DMA2 (3 l/min) was regulated by mass flow controller. The RH of the DMA2 sheath flow was managed to match the humidifier (85% RH). The HTDMA were installed in thermostatic chamber in which temperature was controlled to 25±0.1℃. The total aerosol flow was 0.4 L/min (the sum flow rate of the CPC, 0.3 L/min and the ATOFMS, 0.1 L/min). Aerosol residence time in humidifier was ~10 s. PSL spheres of known size and $(NH_4)_2SO_4$ salt were used to calibrate the HTDMA. The HTDMA uncertainty in GF determination is ±0.05 (Ye et al., 2009;Swietlicki et al., 2008).

2.2. ATOFMS

The schematic of ATOFMS (Model 3800-100, TSI. Inc) is illustrated in Figure 1. Particles were drawn into ATOFMS through a 0.1mm orifice and focused into narrow beam through successive expansions and contractions in the aerodynamic focusing Lens (AFL). Particles leaving the AFL obtain velocities depending on their aerodynamic sizes. In the ATOFMS sizing region particles pass through two orthogonally oriented continuous lasers (Nd: YAG, 532 nm) and laser light was scattered. The scattered light generates pulses in two photomultiplier tubes

(PMT) and the signal delay between the two pulses is used to calculate particle velocity. Particle velocity was also used to trigger ionization laser (Nd: YAG, 266 nm) at exact time to ionize particles. The negative and positive ions generated from particles are recorded by a dual polar time-of-flight mass spectrometer. More details of ATOFMS were described elsewhere (Su et al., 2004).

The ATOFMS data was analyzed within the YAADA toolkit (http://www.yaada.org/). Particles showing similar composition were classified by the adaptive resonance theory-based clustering algorithm (ART-2a) (Song et al., 1999). The ART-2a algorithm parameters were set to: vigilance factor = 0.85, learning rate = 0.05 and number of iterations = 20. The clusters generated by the ART-2a were manully regrouped into major types by considering their common composition patterns. The obtained particle types were labelled by refering previous single particle characterization studies (Spencer et al., 2006;Silva et al., 1999;Sullivan et al., 2007;Gaston et al., 2011;Qin et al., 2012).

2.3. Sampling description

The HTDMA-ATOFMS characterization was carried out at the building of department of environmental science and technology in Fudan university (31°18'N, 121°29'E) from Feb-26 to Mar-7, 2014. Aerosol inlet was installed at the building roof about 6 m above the ground. The Fudan campus was influenced by local emissions sources from transportation, residential, business and cooking activities from surrounding areas which can be viewed as urban environment. A period of ambient ATOFMS data, which persisted from Sep-12 to Sep-28, 2012, was recorded at the same site in Fudan campus. Ambient air quality data of pollutants concentrations ($PM_{2.5}$, O_3, and SO_2) in Shanghai city were provided by Shanghai Environmental Monitoring Center (SEMC).

The sampling procedure was similar to our previous study (Wang et al., 2014). The typical HTDMA GF distributions in this site showed two separated hygroscopicity modes. In 85% RH condition, the two modes were present with respective center GF of 1.05 and 1.45, which were conventionally classified as Near-Hydrophobic (NH) and More-Hygroscopic (MH) modes, respectively (Swietlicki et al., 2008). These modes were normally present elsewhere in China and other areas (Liu et al., 2011;Swietlicki et al., 2008). The HTDMA data suggest that the majority of particles (>97 %) were of GF in 0.9-1.7 range. Consequently, particles in this GF range were characterized by HTDMA-ATOFMS with a GF step of 0.1.

To characterize the desired GFs, the two DMAs in HTDMA were set at certain diameters D_{dry} and D_{RH} according to GF=$D_{\mathrm{RH}}/D_{\mathrm{dry}}$. The HTDMA-ATOFMS system was kept sampling until a sufficient number of particles (> 200) were analyzed by ATOFMS for each GF setting (Table 1). We fixed the DMA1 (D_{dry}) diameter to 250 nm, while the DMA2 diameter (D_{RH}) was set as shown in Table 1. The number of particle spectra in ATOFMS was affected by ambient particle concentrations of certain GF. Since particle concentrations in the downstream of HTDMA were very low, longer sampling were maintained to record sufficient number of spectra in ATOFMS (See the CPC concentrations in Figure S1). The ATOFMS instrument used in this study has size detection range of 100-3000 nm. Considering this, the detection efficiency for 250 nm is expected to be low, as 250 nm is on the lower end of ATOFMS detection range. However, in HTDMA-ATOFMS experiment we selected 250 nm particles, because the concentrations of larger particles were found to decrease further in SMPS size distributions. Therefore, the selection of D_{dry} as 250 nm is a compromise between detection efficiency and particle concentrations (Wang et al., 2014;Herich et al., 2008). With the measured ATOFMS particle numbers and CPC concentrations, the detection efficiency of ATOFMS were calculated to be $\sim 1.6\times 10^{-2}$ at the dry size. In Figure S2 we presented ATOFMS detection efficiencies together with the particle hit rate (hit particles/total sized particles) at different growth factors. Generally, the detection efficiencies suggested variations at different GFs. We found higher detection efficiencies in moderate GF range (1.2-1.4) and higher hit rates in GF<1.3 range, which is probably caused by variations of compositions with GF (Hatch et al., 2014).

2.4. Estimation of ambient particle hygroscopicity

Particles in HTDMA-ATOFMS dataset is comparable to ambient ATOFMS particles. Particle types typically present in HTDMA-ATOFMS study were also preset in ambient ATOFMS studies. Therefore, it is possible to assign similar GF to ambient particles if they have similar composition. The estimation method was firstly performed by evaluating spectra similarities between ATOFMS and HTDMA-ATOFMS dataset (dot products of normalized spectra). The

ATOFMS is known to have higher detection efficiencies toward some metals (such as Na, K, Fe), resulting inappropriately large peaks in particle spectra. We solved the bias by taking the 0.5 power treatment to peaks intensities (Rehbein et al., 2012). In this treatment the larger peaks were suppressed in some degree while smaller peaks increased their weigh relatively. The 0.5 power treatment to peaks intensity was applied because it offered better results in the estimation of hygroscopicity than without it, as discussed in the supplemental information (Figure S3). In the second step we searched matched particles from the HTDMA-ATOFMS dataset showing the best similarities with the ambient particle (dot products in 95-100% range of the maximum dot product). In this study we set a threshold similarity (0.7 dot product) in matching particles, as was required in ART-2a algorithm (Song et al., 1999). Ambient particles with matching dot products <0.7 were excluded from analysis of the estimated GF. The similarity data suggests that 96.2% of the matching similarities are > 0.7 and 79% of them are >0.8 (Figure S4). Since each of the matched particles in HTDMA-ATOFMS dataset was associated with a GF, we obtained a collection of the matching GFs (0.9 -1.7 in 0.1 step). The estimated GF of the ambient particle was determined to be the weighted average of the matched GFs, with the weights being the number percentage of matched particles in each GF bins:

$$GF_{pred} = \frac{\sum GF_i \cdot F_i}{\sum F_i}$$

where: GF_{pred}= the estimated GF of ambient particle, GF_i= GF value from 0.9 to 1.7 interspaced by 0.1, F_i= number percentages of the matched particles in each GF bin.

The estimation process relied on statistical approach in estimating the most probable hygroscopicity for ambient particles, rather than by inferring particle compositions of single particles (Healy et al., 2014). The latter method derived quantitative concentrations of various compositions from peak intensities, which were then applied to predict particle hygroscopicity using the Zdanovskii-Stokes-Robinson mixing rules. Some assumptions including material densities were needed in that method. As a comparison, we inferred hygroscopicity by matching particles with HTDMA-ATOFMS particles of known hygroscopicity. Therefore, the estimated GFs were derived from the measured GF and the assumptions of composition densities and detection sensitivities in ATOFMS are obviated.

The uncertainties in the GF prediction in this method were estimated. The uncertainties in eventual GF may stem from the intrinsic uncertainties in HTDMA-ATOFMS techniques. For the estimation algorithm itself, only few parameters exist that are capable to affect the estimated GF. With the 0.5 power treatment to peak intensities, the only parameter that could influence the estimated GF would be the matching criteria of particles. We have adjusted the matching criteria of 95-100% maximum dot products to 90-100% and 98-100% and the variations in particle GFs were inspected (Figure S5). Based on the variations of the obtained GF, we estimated that the uncertainty in GF estimation is within ±0.15.

3. RESULTS AND DISCUSSIONS

3.1. Single particle composition and hygroscopicity in HTDMA-ATOFMS experiment

3.1.1 Hygroscopicity distribution of different particle types

The particles in the HTDMA-ATOFMS dataset were classified into major types based on their mass spectra. The ART-2a algorithm was applied to particle clustering and then similar clusters were combined. The majority of particles were eventually classified into 9 types including Biomass, Fresh EC, Aged EC, Dust/Ash, HMOC, Amine-rich, Ammonium/OC, Cooking and Sea salt. In Figure 2 we present the average spectra of each type and their numbers detected in each GF bin. Since the total number of detected particles in GF bins were not equal (Table 1), we also present the particle numbers normalized by the total numbers to indicate their detection probability in each GF bin (Figure. 2). The hygroscopicity of particle types showed different distribution patterns with GF. The hygroscopicity characters of Biomass, EC, Dust/ash, HMOC and Amine-rich types were described previously and their hygroscopicity have shown consistent trend with the previous characterization (Wang et al., 2014).

The Biomass particles produced characteristic peaks of -26(CN), -42(CNO), -59($C_2H_3O_2$), -73($C_3H_5O_2$) and dominant peak at 39K and related peaks at 113(K_2Cl) or 213(K_3SO_4) (Silva et al., 1999;Zauscher et al., 2013;Pratt and Prather, 2009). Biomass particles displayed low hygroscopicity since majority of them were present in GF <1.2 range, with the peak detection probability at GF 1.1 (Figure 2 (a)). The hygroscopicity of Biomass particles is consistent with other HTDMA measurement of biomass particles (Rissler et al., 2006;Laborde et al., 2013).

The hygroscopicity of biomass particles in ambient environment were similarly detected in the HTDMA-SP2, which suggested the center GF of 1.1~1.2 of biomass particles (at 90% RH), corresponding to the GF of 1.06-1.13 at 85% RH (Laborde et al., 2013).

The EC particles were detected by a series of elemental carbon peaks at C_n (n=1, 2, 3 …) in the negative and positive spectra (Ault et al., 2010;Spencer et al., 2006;Toner et al., 2008). EC particles distributed broadly from nearly-hydrophobic (NH) mode to more-hygroscopic (MH) mode. However, the mass spectra of hydrophobic and hygroscopic EC particles were different in their mass spectra. As shown in Figure 2 (b-c), The mass spectra of hygroscopic EC particles produced stronger secondary peaks (-62NO_3^-, -97HSO_4^-, 18NH_4^+) than hydrophobic EC particles, consistent with the significant fractions of secondary matters in hygroscopic EC (Laborde et al., 2013). According to their hygroscopicity distributions, the general EC type was divided into Fresh EC and aged EC type. The mass spectra of Fresh EC suggested they were freshly emitted without significant secondary coatings (Weingartner et al., 1997;Laborde et al., 2013;Herich et al., 2009). Peak intensity trends of 62NO_3^-, -97HSO_4^-, 18NH_4^+ and other related peaks at different GF were summarized for EC particles (Figure S6). Based on the statistics of peak intensities, we found clear increasing trends of secondary peak intensities in GF 0.9-1.2 range, but not in all GFs (Laborde et al., 2013;Herich et al., 2008).

Dust/ash type particles produced inorganic peaks of salts and metals (Gaston et al., 2017;Ault et al., 2011;Sullivan et al., 2007). Most of dust/ash particles were detected in hygroscopic range (GF>1.3). Most of Dust/ash particles were internally mixed with nitrate. Within the general Dust/ash type there are many sub-clusters according to specific association of metal peaks in particle spectra. Some of the clusters showed characteristic hygroscopicity distributions which offered values in the source apportionment of these particles. As an illustration, we presented the mass spectra and hygroscopicity distribution of the Al-Si cluster in Figure 3. The mass spectra of Al-Si particles showed stronger aluminum (27Al^+) and silicate (-76SiO_3^-) peaks in their positive and negative spectra, respectively. Particle number distribution of Al-Si particles suggested that they were detected with the highest probability at GF 1.1. In the preliminary study we identified the similar Al-Si particles exclusively in NH mode (Wang et al., 2014). Based on their hygroscopicity distribution, we assumed the Al-Si particles are soil dusts according to their reported low hygroscopicity (Koehler et al., 2009).

The spectra of HMOC particles showed obvious organic peaks in higher m/z range (>150). Some HMOC particles produce obvious polycyclic aromatic hydrocarbons (PAH) peaks in positive spectra and high mass signals in negative spectra. The mass spectra of HMOC suggested they were generated from combustion including traffic emissions (Dall'Osto et al., 2013;Toner et al., 2008). The majority of HMOC particles displayed low hygroscopicity (GF<1.2) (Wang et al., 2014;Herich et al., 2008).

Amine-rich type particles produced amine peaks at +59(C_3H_9N), +86($C_5H_{12}N$) and +101($C_6H_{15}N$) (Angelino et al., 2001;Pratt et al., 2009). Particulate amine formation was favored in low temperatures and higher humidity conditions (Huang et al., 2012;Zhang et al., 2012). The elevated amine particle fractions may be related to the low temperature (6 °C) and high humidity (78% RH) condition during this experiment. Both the preliminary and present study identified the hydrophilicity of Amine-rich particles, with the highest number contributions to GF>1.5 range (Wang et al., 2014). Short alkyl chain aliphatic amines are known to have relatively high vapor pressures and basic in nature, their presence in particles indicates they are most likely occur in the form of aminium salts, whose formation is greatly favored in the presence of particulate water (Angelino et al., 2001;Chen et al., 2019). Mass spectra of Amine-rich particles suggest that 77% of them were internally mixed with sulfate or nitrate.

With the expanded GF range and sampling durations, we identified other particle types of specific hygroscopic patterns, including Ammonium/OC, Cooking and Sea salt particles in this study. The Ammonium/OC particles demonstrated some similarities with biomass particles. There was predominant potassium peak ^{39}K and many organic peaks in the positive mass spectra, as shown in Figure 2. Additionally, stronger $18NH_4^+$ peaks for ammonium and sulfate ($-97HSO_4$) were also present in these particles. The typical $-26CN^-$ and $-42CNO^-$ peaks observed for biomass particles were absent or very weak, suggesting the composition differences between Ammonium/OC and biomass particles (Silva et al., 1999;Zauscher et al., 2013;Pratt and Prather, 2009). The hygroscopicity of the Ammonium/OC particles was unique since they have the largest contributions to moderate GF range (GF 1.1-1.3), with the maximum contribution found at GF=1.2. The GF of Ammonium/OC particles suggests that they can be categorized as LH mode (Swietlicki et al., 2008). A prior ATOFMS study identified that Ammonium/OC particles were from agricultural sources, and found most of them were present in higher photochemical oxidation periods (Qin et al., 2012), consistent with the prominent secondary peaks of ammonium found in this study. It is likely the organics in this type is secondary since the GF 1.2 is close to the hygroscopicity of SOA (GF=1.24 at 90% RH) (Gysel et al., 2007;Sjogren et al., 2008). We inferred that ammonium was not contributing major fractions to Ammonium/OC particles, since ammonium salts was very hydrophilic while Ammonium/OC demonstrate only moderate hygroscopicity.

Cooking is an important source of primary organic aerosol (POA) in urban regions (Crippa et al., 2013;Dall'Osto and Harrison, 2012). Zhang et al. estimated that up to 35% of POA are attributed to cooking aerosol during meal hours (Zhang et al., 2007). Cooking particles around the site was likely to be significant considering that the Fudan campus is located in a heavily populated area. The ATOFMS characterization of cooking particles have been performed previously (Dall'Osto et al., 2013). The marker peaks at -255($C_{16}H_{32}O_2$, palmitic) and -281 ($C_{17}H_{34}O_2$, oleic acid) in the negative spectra were used to identify Cooking particles (Dall'Osto and Harrison, 2012;Silva, 2000). As shown in Figure 2(h), Cooking particles demonstrated very low hygroscopicity and were detected exclusively in GF<1.1 range. It is noted that GF 0.9 does not necessarily indicate a particle shrinkage in 85% RH. Cooking particles might become more spherical in elevated RH, resulting in smaller mobility diameters. This phenomenon was observed for other organic particles (Shi et al., 2012;Pratt and Prather, 2009). The low hygroscopicity of cooking particles is consistent with the enriched organic as indicated by the fatty acids (-171, -255, -279, -281) and HOA (+55, +57) peaks in the spectra. The detection of cooking particles in NH mode complemented to the conclusion that combustion processes are mainly responsible for NH particles (Swietlicki et al., 2008;Laborde et al., 2013;Herich et al., 2009).

With particles of higher GF being analyzed in this experiment, we also identified the Sea salt particle which constitutes an important particle type in ambient air in coastal areas (Herich et al., 2009;Gard et al., 1998). Sea salt mass spectra contain dominant sodium peak 23Na^+ and other sodium cluster peaks at 62Na_2O^+, 63Na_2OH^+, 81Na_2Cl^+ (Gaston et al., 2017). The hydrophilicity of Sea salt is clear that they were mostly detected in the largest GF bins (>1.5), with their number fractions increased from GF 1.5 to 1.7 (Figure. 2). HTDMA studies in marine environment shown that sea salt particles constitute a separated hygroscopicity mode of the largest GF (Swietlicki et al., 2008), which is generally consistent with the observed GF range in the experiment. However, the observed sea salt particle hygroscopicity is somewhat different from the HTDMA-ATOFMS characterization in a subarctic region, where sea salt particles were found mainly detected in GF 1.3-1.5 range at 82% RH (Herich et al., 2009). We inferred that sea salt hygroscopicity properties are variant with locations and other factors (organics in seawater, marine microbiological conditions, aging) should be considered (Facchini et al., 2008;Randles et al., 2004).

3.1.2 Peak intensity variations with GF

Apart from particle number distributions, the HTDMA-ATOFMS dataset provided another aspect of information regarding peak intensities with GF. In this study, we used relative peak intensities (peak areas normalized by the total areas in spectrum) to investigate its relation to GF. Generally, the responses of peak intensity to GF variation were found to be nonlinear, since they were correlated only within specific GF ranges. A simple trend applicable to whole GF range was not observed.

We presented the statistics of peak intensity of nitrate (46NO_2^-, 62NO_3^-, 125$H(NO_3)_2^-$) and sulfate (80SO_3^-, 97HSO_4^-) which were known to be critical to particle hygroscopicity (Figure 4). As previously observed, the nitrate and sulfate peaks were present in the majority of particles in all GF bins (Herich et al., 2009;Herich et al., 2008;Wang et al., 2014). However, peak intensities of nitrate and sulfate were indeed stronger in hygroscopic particles than hydrophobic particles. In Figure 4 we observed positive correlation between nitrate and sulfate intensities and GF in GF <1.2 range, suggesting contribution of nitrate and sulfate to particle hygroscopicity in low GF range (Figure 4). However, in higher GF range (GF 1.3-1.5), nitrate and sulfate peaks seem to reach a plateau with unclear dependence on GF. Nitrate and sulfate were known to contribute large fractions of particle mass in MH particles (Swietlicki et al., 2008;Laborde et al., 2013;Liu et al., 2014). The unclear trend of nitrate and sulfate with GF seem to suggest that nitrate and sulfate were in stable ratios since nitrate and sulfate peaks were dominating peak areas in negative spectra. For particles of even higher GF, differences were observed between GF 1.3-1.5 and GF 1.5-1.7 range in that stronger nitrate and weaker sulfate peaks were detected in the GF 1.3-1.5 range. Particles classification suggests that this general characteristic is also at variance for different particle types. The same statistics for EC and Dust/ash particles were presented in Figure 4. Compared with EC particles, smaller sulfate and stronger nitrate peaks were found in Dust/ash spectra, and the observed trend in total particles were less obvious in Dust/ash. These facts highlight the nonlinearity between peak intensities and GF and that particle types should also be considered in describing peak intensities.

The analysis of peak intensities with GF can disclose some atmospheric processes happened on aerosol. We take the Sea salt as an illustration. Sea salt particles were known to react with atmospheric nitric acid, with NaCl in fresh sea salt be transformed into $NaNO_3$ in the reacted sea salt (Gard et al., 1998). This composition transformation is indicated in corresponding changes of NaCl and $NaNO_3$ peak intensities in particle spectra. The unreacted sea salt particles tend to produce larger peaks of Na_2Cl^+ and $NaCl_2^-$ in spectra (Gaston et al., 2011;Prather et al., 2013). In particle spectra of reacted sea salt, the NaCl peaks (Na_2Cl^+, $NaCl_2^-$) decrease while $NaNO_3$ peaks ($Na_2NO_3^+$, $Na(NO_3)_2^-$) increase. We presented peak intensities of sea salt in GF 1.5-1.7 range where sea salt particles were detected with largest numbers (Figure 5). We found that the positive correlation between NaCl peak intensity and GF, and the negative correlation for $NaNO_3$ peaks. Therefore, the HTDMA-ATOFMS data supported that reacted sea salt have reduced hygroscopicity (Herich et al., 2009;Gaston et al., 2018). Laboratory HTDMA study suggested that NaCl and $NaNO_3$ have deliquesced at 85% RH and that the $NaNO_3$ (GF ~1.8) is less hygroscopic than NaCl (GF ~2.2) (Hu et al., 2010). The reduced hygroscopicity of sea salt is in line with the GF of sodium salts. However, the sea salt hygroscopicity (GF 1.5-1.7) was smaller than pure $NaNO_3$ salt (supposing fully reacted), suggested that the chemical transformation alone is not sufficient to account for the observed hygroscopicity of sea salt. We hypothesize that other compositions as organics were mixed into sea salt and contributed to the reduction of sea salt hygroscopicity (Gaston et al., 2011;Randles et al., 2004;Facchini et al., 2008).

3.2 Predictability of hygroscopicity from particle mass spectra

The GF of a particle can be estimated based on HTDMA-ATOFMS data for two reasons. First, different particle types had distinct GF distributions. Second, particles in different GF bins had different mass spectra. The GF estimation from particle spectra requires that the HTDMA-ATOFMS data is capable to represent the major particle types normally presented in atmosphere, which is evidenced in the preceding discussions. In another aspect, the GF prediction from mass spectra also demands that HTDMA-ATOFMS data are sensitive to reflect the composition differences with GF variations.

To test the sensitivity of HTDMA-ATOFMS data, we evaluated the average spectral similarities between each pair of GF groups. The average similarities were calculated from the similarities between every possible pairs of particles from the two GF groups. The self-comparing of particles within the same GF group were excluded. As shown in Figure S7, we observed a general trend that particles in the same GF bins tend to produce the highest similarities. As the GF differences increase, the mass spectra similarity between two GF bins tended to decrease. This result is an evidence that the particles with different GFs are more likely to have discriminable mass spectra, which suggests that the HTDMA-ATOFMS dataset are capable to estimate hygroscopicity just from particle mass spectra.

3.3 Estimated hygroscopicity of ambient particles

A case study of the hygroscopicity estimation were carried out based on a period of ambient ATOFMS measurement. The ATOFMS data was collected at the same Fudan site from Sep-12 to Sep-28, 2012. During this period the ATOFMS recorded 538,983 mass spectra of individual particles. With the described estimation method, the GF value (corresponding to 85% RH) was generated for each particle based on individual particle mass spectra. A fraction of the estimated GF (4%) were excluded from analysis since their maximum similarities failed to exceed the threshold value (dot product > 0.7) between ATOFMS and HTDMA-ATOFMS particles. Particle mixing states in this period were analyzed by clustering particles using ART-2a algorithm (Song et al., 1999). After merging the clusters of similar composition and temporal trends, the majority of particles were finally grouped into the same general types as discussed in HTDMA-ATOFMS dataset (Fresh EC, Aged EC, Dust/Ash, HMOC, Amine-rich, Ammonium/OC, Cooking and Sea salt), which account for 90.8% of the total analyzed particles in this period.

3.3.1 Hygroscopicity modes and contributions from particle types

The estimation method determined that the GF of ATOFMS particles were restricted within the GF range in HTDAM-ATOFMS dataset (0.9-1.7). Within this GF range, the ATOFMS particle GF distribution suggested several hygroscopicity modes similar to the HTDMA measurement. As shown in Figure 6, three hygroscopicity modes were clear in the GF-number distributions, with particle GF centered at about 1.05, 1.42, and 1.6, respectively (85% RH). Prior HTDMA studies suggested the regular presence of the nearly-hydrophobic mode with center GF in 1.05~1.1 range in Shanghai area (Ye et al., 2011), consistent with the GF 1.05 mode in this study. The second mode at GF 1.42 mode in ATOFMS particles corresponds to the MH mode (GF 1.43~1.47) in Shanghai and other sites using HTDMA (Ye et al., 2013;Ye et al., 2011;Liu et al., 2011). The sea salt mode in HTDMA GF distribution is not always clear because of the larger size of sea salt particles. However, the sea salt particles were readily detected by ATOFMS because of the detection range of ATOFMS. The particles in GF 1.6 mode contained rich sodium content and their mass spectra suggest typical sea salt peaks (Figure S2). In marine areas the sea salt particles were found to constitute hygroscopicity mode of the largest GF (about 2.0 at 90% RH, corresponding to 1.76 at 85% RH) (Swietlicki et al., 2008).

The ATOFMS measured particle aerodynamic diameters simultaneously for individual particles. Together with the estimated GF, we inspected particle number distribution as a bivariate function of the estimated GF and diameter (aerodynamic diameter, d_{va}) (Figure 7). The hygroscopicity modes were clearer in the GF-d_{va} diagram, which suggest the increasing trend of particle diameter with increasing GF, a very consistent result with HTDMA studies (Ye et al., 2011;Ye et al., 2013). Healy et.al. applied a different method to estimate particle hygroscopicity from single particle data using ZSR mixing rule (Healy et al., 2014). The particle aerodynamic diameter d_{va} was transformed to equivalent mobility diameter d_m by assuming a particle density in that study. Although the methods are different, the identified hygroscopicity modes were similar between the two studies, except the sea salt mode which was not found by Healy et al. (Healy et al., 2014).

Based on the GF of hygroscopicity modes, prior HTDMA studies conventionally classified the observed modes into categories as nearly-hydrophobic (NH), less-hygroscopic (LH), more-hygroscopic (MH) and sea salt (SS) modes respectively (Swietlicki et al., 2008;Liu et al., 2011;Sjogren et al., 2008). However, the chemical nature of these hygroscopicity modes was not clear since the HTDAM technique is based on particle numbers and the particle composition information was not obtainable. With the ATOFMS single particle data, particle composition and hygroscopicity was connected directly. To facilitate comparison, we similarly divide the estimated GF into four bins (<1.1, 1.1-1.3, 1.3-1.5 and >1.5) to roughly represent the NH, LH, MH, SS particles according to the conventional classification of hygroscopicity modes (Swietlicki et al., 2008). As shown in Figure 6, particle types were distributed differently in GF modes. For example, the organic particles including HMOC, Biomass and Freshly emitted EC particles were mainly enriched in NH mode, which suggests directly that combustion sources are mainly responsible for NH particles in the ambient (Herich et al., 2008;Herich et al., 2009;Ye et al., 2011).

In Table 2 we made the statistics on average number contributions of particle types to the NH, LH, MH and SS mode. The presented statistics were based on the temporal contributions of each particle types in daily resolution. It is noted that particle number contributions presented in Table 2 may be different from HTDMA-ATOFMS dataset (Figure 2). For example, the Cooking particles contributions to NH mode was significantly lower in the ATOFMS dataset (3%) than HTDMA-ATOFMS dataset (19%). This result is understandable because particle concentrations are variant with particle size and HTDMA-ATOFMS only analyzed a narrow size bin from the total particle size distribution. For each hygroscopicity mode, there were multiple particle types contributing significant number fractions, suggesting that even within the same hygroscopicity mode there were still some heterogeneity in particle composition. Particles in the same hygroscopicity mode may share some common features in compositions but their differences are distinguishable in single particle data. In another respect, the contributions of each type also suggest the existence of a predominant type that accounts for major fractions in respective modes compared with other types, such as Aged EC in MH mode, Ammonium/OC in LH mode. The comparison between Table 2 and Figure 2 suggests that, although their absolute contributions may be different, the hygroscopicity patterns of particle types in the two datasets are in good agreement. Based on this fact, we concluded that the composition-hygroscopicity connections contained in HTDMA-ATOFMS dataset was successfully reflected into the predicted GF.

3.3.2. Temporal variations of estimated hygroscopicity

The temporal variation of particle estimated GF from Sep-12 to Sep-28 was illustrated in Figure 8. Four distinct periods (P1-P4) were identified based on their different hygroscopicity distributions. Generally, the P1 and P3 periods were characterized by elevated MH mode which dominated the ATOFMS particles numbers, while in P2 and P4 the MH particles decreased significantly and sea salt mode was pronounced. Back trajectories during P1-P4 were analyzed using HYSPLIT mode (Draxler, R. R. and Rolph, G. D., 2003) to inspect the airmass that influenced the sampling site (Figure S9). The 24-hour back trajectories suggests that the airmass in P1 period mainly circulated in local regions from northwest direction to Shanghai. The local circulations brought regional aerosol pollution to the sampling site, resulted in elevated concentrations of particles, especially the MH particles. During P2, the airmass originated from the ocean in northeast direction with less continental influence. The cleaner air from the ocean almost wiped out the accumulated particles observed in P1 and the concentrations of sea salt particles increased. In the majority of time during P3, the airmass stayed over continental areas. The MH particles dominated particle numbers in this period and the sea salt mode were barely present. During Sep-18 to Sep-20 in P3, the LH particles showed increased concentrations and gradually decreased after Sep-20. Similar to P1, the origin of airmass in P4 shifted to the ocean in eastern directions and SS mode emerged again. Both the particle spectra and the back trajectories supported that the GF mode of 1.6 can be mainly attributed to sea salt particles.

Except meteorological conditions, other differences exist in the temporal trends for each hygroscopicity modes. Generally, the NH mode showed relatively stable trends irrespective of different periods of P1-P4, as indicated in Figure 8. Closer inspection of NH particles suggests a notable feature that obvious sharp spikes were present in NH particle temporal concentrations (Figure 8). This character is typical for particles from local emission sources, with undissipated plumes at the time of detection. With the combined information from particle composition in

Table 2, we inferred that the NH particles were fresh emitted particles from local sources with high organic or elemental carbon content (Laborde et al., 2013;Herich et al., 2008;Weingartner et al., 1997). The mass spectra of NH particles indicated low nitrate and sulfate signals, suggesting that secondary matters have not accumulated significantly on these particles, consistent with negligible coating thickness on NH particles (Laborde et al., 2013). We tend to ascribe the organics in NH particles to be primary organic carbons (POA) considering their relatively fresh emission state (Sjogren et al., 2008;Liu et al., 2011;Gysel et al., 2007).

Some characters of LH particles were noticed. Similar to the particles in MH range, the LH particles mainly presented in continent influenced periods (P1 and P3) (Figure 8). However, the temporal concentrations trends suggested differences between LH and MH particles. For example, MH mode dominated particle numbers in the entire P3, while the LH particles were only pronounced from Sep-17 to Sep-21, with peak concentrations observed on Sep-19. The particle contributions showed that Ammonium/OC is the main contributor to NH particles (Table 2). This conclusion is also correct in temporal basis since the Ammonium/OC contributions to LH range were always much larger than other types of particles in all the studied period. We investigated the nature of the Ammonium/OC particles by comparing its concentration with ambient pollutants levels. As shown in Figure 9, the number fractions of Ammonium/OC particles showed strong connections to ambient O_3 concentrations. During Sep-17 to Sep-21 there were daily oscillations of O_3 levels, which were followed by the same pattern of Ammonium/OC particles with lags of several hours. The maximum O_3 concentrations was found on Sep-19 (219 μgm^{-3}) in the period, the same day when the highest Ammonium/OC particle contribution was observed. HTDMA studies suggested that LH mode became pronounced in new particle formation (NPF) periods with high atmospheric reactivity (Swietlicki et al., 2008). Based on these facts, we think the Ammonium/OC particles were related to the oxidation processes of organics vapors by oxidants such as O_3 (Varutbangkul et al., 2006). The moderate hygroscopicity of Ammonium/OC agrees with the hygroscopicity of ambient secondary organic aerosol (SOA) (Gysel et al., 2007;Sjogren et al., 2008). During periods of higher Ammonium/OC contributions (Sep-17 to Sep-21), increased SO_2 levels were also encountered, which coincided with high sulfate signals in mass spectra of Ammonium/OC

(Figure 2). Compared with the organic compositions, the sulfate was inferred to have minor contributions to mass fractions because of the moderate hygroscopicity of Ammonium/OC.

Particles in MH mode dominated the particle numbers for the majority of time in P1 and P3 (60%) compared with the average fraction of 25% in P2 and P4. Inspection of the temporal trends of MH particles also suggest some diurnal variations with higher concentrations in nighttime (Figure 8). As illustrated in Figure 4 and Figure S6, mass spectra of MH particles were dominated by sulfate, nitrate peaks, suggested that MH particles were mixed with significant fraction of secondary inorganic matters (SIA). The coating thickness of the secondary matters was determined by HTDAM-SP2 at different GF (Laborde et al., 2013). The coating thickness of secondary coating was measured to 40-80 nm (D_{dry}=265 nm) in GF 1.2-1.7 range, being equivalent to 55-76% of hygroscopic particle volume was attributed to secondary matters (Laborde et al., 2013;Healy et al., 2014).

3.3.3 Peak intensity variations with estimated GF

Particle hygroscopicity and peak intensities in particle mass spectra were correlated to show their connections. The correlation was illustrated similarly to the analysis of the HTDMA-ATOFMS dataset, as shown in Figure 10. In addition to the statistics on peak intensities of different GF, the number distributions ATOFMS particles with GF and peak intensities were presented for nitrate ($46NO_2^-$, $62NO_3^-$, $125H(NO_3)_2^-$) and sulfate peaks ($80SO_3^-$, $97HSO_4^-$,) in the lower panels in Figure 10. The general trends of peak intensities with GF in HTDMA-ATOFMS dataset was preserved in estimated GF of ambient particles. The trends of nitrate and sulfate peak intensities showed increases from NH to LH range and remained constant in the MH mode. Similar to HTDMA-ATOFMS particles, stronger nitrate peaks were detected in SS particles compared with the MH particles, while an opposite trend was observed for sulfate intensities. These results highlight the nonlinearity between GF and peak intensities of ATOFMS particles.

The nonlinearity of peak intensities with GF was also suggested by the different particle types presented in ATOFMS data. As shown in the lower panels in Figure 10, the distribution of ATOFMS individual particles showed enrichment in different areas in the GF-peak intensity diagram, suggesting the presence of particle groups of different compositions. To illustrate this character, we selected two areas with clear particle enrichments in GF-peak intensity diagram and their particle composition were analyzed (denoted as A and B in lower left panel in Figure 10). Obviously, particles in area A produced much larger nitrate signals than particles in area B. Particle numbers in the two areas suggested that Dust/ash dominated particles in area A (59%) while in area B the Dust/ash only accounted for 14% of particles (Figure S10). As a contrast, particles in area B were dominated by Aged EC type (53%) followed by 25% Dust/ash. Table 2 suggests that Aged EC and Dust/ash are the major types presented in the same MH mode. However, peak intensity responses to GF were indeed different for different particle types, suggesting the importance of particle types in describing peak intensities.

The particle distribution with sulfate intensities showed similar enrichment patterns to nitrate (lower right panel in Figure 11). Sulfate peak intensities were found to correlated with hygroscopicity in GF <1.2 range but in MH range no correlated with GF was observed. We note that except the larger peaks of nitrate and sulfate, some smaller peaks were also found to correlated with GF within specific particle type. We correlated peak intensities of Na_2Cl^+ and NO_3^- with the estimated GF of sea salt particles (Figure S11). The Na_2Cl^+ peaks were positively correlated with GF while the nitrate peaks were negatively correlated with GF. The observed correlation in sea salt particles are consistent with discussed trends in the HTDMA-ATOFMS dataset. These results demonstrate that the GF estimation method have effectively reflected the minor changes in particle mass spectra into the estimated hygroscopicity.

3.3.4 Comparing the estimated hygroscopicity with visibility

Particle optical properties were closely connected to hygroscopicity (Liu et al., 2012;Qu et al., 2015;Chen et al., 2012). The hygroscopic growth increases particle volumes and cross sections and is contributing to the visibility degradation. With the estimated hygroscopicity of ATOFMS particles, we correlated atmospheric visibility with particle concentrations to study their contributions to the visibility variation. The ATOFMS particle volume concentrations were calculated for hygroscopicity modes of NH, LH, MH and SS based on ATOFMS particle diameter and numbers. The particle volume concentrations was used because hygroscopic growth change particle sizes rather than numbers (Chen et al., 2012). The visibility data was obtained from (https://www.wunderground.com/) logged in the Hongqiao airport (31°12' N, 121°20' E) and Pudong airport (31°9.3' N, 121°49' E) during the study period (see the map in Figure S12). The temporal variations of visibility in two sites correlated strongly (Figure S12), despite the 45 kilometers distance between two airports. The Fudan site is located roughly between the two airports, and the two sets of visibility data were averaged to represent the study site. In P2 and P4 the site was under the influences from ocean, resulting visibilities larger than 10 km (Figure 8). Apart from ATOFMS particles, contemporary $PM_{2.5}$ volume concentrations were also correlated with visibility. The $PM_{2.5}$ volume concentrations were derived from $PM_{2.5}$ mass concentrations using particle density (1.4 gcm^{-3}). A strong correlation between ATOFMS particle numbers and $PM_{2.5}$ was found (R^2=0.80).

An exponential relation between visibility and PM concentrations was found by the previous study (Qu et al., 2015). After applying the exponential fitting to the visibility and particle volume concentrations, we found a moderate correlation for ATOFMS particles (R^2=0.45) and better correlations for $PM_{2.5}$ concentrations (R^2=0.64) (Figure S13). However, the fitting errors were clearly dependent on ambient RH, with larger errors in higher humidity, indicating that hygroscopicity might affect visibility degradations, which were consistent with other studies (Chen et al., 2012;Liu et al., 2012). To further examine the effect of particle hygroscopicity on visibility, we derived particle volumes in different RH using estimated κ values (Petters and Kreidenweis, 2007). The κ values were calculated using the GF of individual particles at 85% RH for ATOFMS data and the average GF of 1.36 for $PM_{2.5}$ volume data. With hygroscopicity being considered, we found notable improvements of the correlations between PM concentrations and visibility, with the improved correlation observed for $PM_{2.5}$ concentrations (R^2=0.82) after applying correction for hygroscopicity (Figure 11). However, this improvement was barely the case for NH particles, probably due to the negligible hygroscopic growth. For the ATOFMS particles in different GF modes, we found the highest R^2 (0.65) for the MH particles. The correlation between SS particles and visibility was distorted due to the visibility reached its limit (10 km) when sea salt mode was pronounced (Figure 8). The R^2 between MH particles and visibility suggests that the variation of MH particles accounted for the major part of visibility changes (65%) during this period, which coincided with the major contribution of nitrate and sulfate to light extinction (61%) in eastern China areas (Qu et al., 2015). These results indicate the importance of discriminating particles by hygroscopicity in explaining the measured visibility.

4. CONCLUSIONS

The hygroscopicity and composition of submicron particles were characterized in a megacity in eastern China. A single particle mass spectrometer was connected to the downflow of an HTDMA to analyze particle composition of different hygroscopicity at 85% RH. Direct connections between hygroscopicity and single particle signatures were established. The HTDMA-ATOFMS dataset suggested that particle types were distributed differently in various hygroscopicity ranges. Generally, Fresh EC particles and organic particle types including Biomass, Cooking and high molecular organic carbon (HMOC) were enriched in nearly-hydrophobic (NH) mode (GF<1.1). The majority of particles in NH mode suggested characters of freshly emitted particles from combustion sources. Particle types in the more-hygroscopic (MH) range (GF1.3-1.5) include Aged EC, Amine-rich and Dust/ash particles. The mass spectra of MH particles suggested that they were mixed with significant fractions of secondary matters. The sea salt particles were detected in the higher GF range (GF 1.5-1.7), with increasing detection probability at larger GF. In the moderate hygroscopicity range (GF 1.1-1.3), the Ammonium/OC particles was identified with peak detection probability at GF 1.2.

Single particle spectra peak intensities were correlated with GF to disclose their possible connections. The peak intensities were nonlinearly correlated with GF. The peak intensities of nitrate and sulfate showed gradual increase from GF 0.9 to 1.2 while in larger GF range the same trends were not observed. Peak intensities showed opposite directions for nitrate and sulfate in GF 1.5-1.7 range with stronger nitrate peaks and smaller sulfate peaks. Except the general nonlinearity of peak intensities is subjected to variations with different particle types. The peak intensity analysis suggested the reduced hygroscopicity of sea salt after atmospheric aging.

Based on the established connections between composition and composition, we developed a method to estimate particle hygroscopicity from single particle mass spectra. The method was tested in a period of ATOFMS data in Shanghai. The estimated GF of individual particles suggested that ATOFMS particles were present in similar hygroscopicity modes as HTDMA measurement on ambient aerosol. We discriminated particles into NH, LH, MH and SS mode by the GF of individual particles. Particle type contributions to the these hygroscopicity modes suggested consistent results with HTDMA-ATOFMS dataset. Based on the combined information on particle composition, hygroscopicity and airmass back trajectories, we inferred that the POA/EC, SOA, SIA and salts are the characteristic compositions for particles in the NH, LH, MH, SS modes, respectively. The proposed method is a novel way of single particle mass spectrometry data analysis, which would provide additional information to the study of particle mixing states, source identification and visibility degradation.

REFERENCES

Angelino, S., Suess, D. T., and Prather, K. A.: Formation of aerosol particles from reactions of secondary and tertiary alkylamines: Characterization by aerosol time-of-flight mass spectrometry, Environmental Science & Technology, 35, 3130-3138, 10.1021/es0015444, 2001.

Ault, A. P., Gaston, C. J., Wang, Y., Dominguez, G., Thiemens, M. H., and Prather, K. A.: Characterization of the Single Particle Mixing State of Individual Ship Plume Events Measured at the Port of Los Angeles, Environmental Science & Technology, 44, 1954-1961, 10.1021/es902985h, 2010.

Ault, A. P., Williams, C. R., White, A. B., Neiman, P. J., Creamean, J. M., Gaston, C. J., Ralph, F. M., and Prather, K. A.: Detection of Asian dust in California orographic precipitation, Journal of Geophysical Research-Atmospheres, 116, 10.1029/2010jd015351, 2011.

Buzorius, G., Zelenyuk, A., Brechtel, F., and Imre, D.: Simultaneous determination of individual ambient particle size, hygroscopicity and composition, Geophysical Research Letters, 29, 1974, 10.1029/2001gl014221, 2002.

Chen, J., Zhao, C. S., Ma, N., Liu, P. F., Gobel, T., Hallbauer, E., Deng, Z. Z., Ran, L., Xu, W. Y., Liang, Z., Liu, H. J., Yan, P., Zhou, X. J., and Wiedensohler, A.: A parameterization of low visibilities for hazy days in the North China Plain, Atmospheric Chemistry and Physics, 12, 4935-4950, 10.5194/acp-12-4935-2012, 2012.

Chen, Y., Tian, M., Huang, R.-J., Shi, G., Wang, H., Peng, C., Cao, J., Wang, Q., Zhang, S., Guo, D., Zhang, L., and Yang, F.: Characterization of urban amine-containing particles in southwestern China: seasonal variation, source, and processing, Atmospheric Chemistry and Physics, 19, 3245-3255, 10.5194/acp-19-3245-2019, 2019.

Cheng, Y. F., Wiedensohler, A., Eichler, H., Heintzenberg, J., Tesche, M., Ansmann, A., Wendisch, M., Su, H., Althausen, D., Herrmann, H., Gnauk, T., Bruggemann, E., Hu, M., and Zhang, Y. H.: Relative humidity dependence of aerosol optical properties and direct radiative forcing in the surface boundary layer at Xinken in Pearl River Delta of China: An observation based numerical study, Atmospheric Environment, 42, 6373-6397, 10.1016/j.atmosenv.2008.04.009, 2008.

Crippa, M., DeCarlo, P. F., Slowik, J. G., Mohr, C., Heringa, M. F., Chirico, R., Poulain, L., Freutel, F., Sciare, J., Cozic, J., Di Marco, C. F., Elsasser, M., Nicolas, J. B., Marchand, N., Abidi, E., Wiedensohler, A., Drewnick, F., Schneider, J., Borrmann, S., Nemitz, E., Zimmermann, R., Jaffrezo, J. L., Prevot, A. S. H., and Baltensperger, U.: Wintertime aerosol chemical composition and source apportionment of the organic fraction in the metropolitan area of Paris, Atmospheric Chemistry and Physics, 13, 961-981, 10.5194/acp-13-961-2013, 2013.

Dall'Osto, M., and Harrison, R. M.: Urban organic aerosols measured by single particle mass spectrometry in the megacity of London, Atmospheric Chemistry and Physics, 12, 4127-4142, 10.5194/acp-12-4127-2012, 2012.

Dall'Osto, M., Ovadnevaite, J., Ceburnis, D., Martin, D., Healy, R. M., O'Connor, I. P., Kourtchev, I., Sodeau, J. R., Wenger, J. C., and O'Dowd, C.: Characterization of urban aerosol in Cork city (Ireland) using aerosol mass spectrometry, Atmos. Chem. Phys., 13, 4997-5015, 10.5194/acp-13-4997-2013, 2013.

Draxler, R. R. and Rolph, G. D., HYSPLIT (Hybrid Single-Particle Lagrangian Integrated Trajectory) model v 4.9, NOAA Air Resource Laboratory, Silver Spring MD, available at:

http://www. arl.noaa.gov/ready/hysplit4.html, 2019.

Facchini, M. C., Mircea, M., Fuzzi, S., and Charlson, R. J.: Cloud albedo enhancement by surface-active organic solutes in growing droplets, Nature, 401, 257-259, 10.1038/45758, 1999.

Facchini, M. C., Rinaldi, M., Decesari, S., Carbone, C., Finessi, E., Mircea, M., Fuzzi, S., Ceburnis, D., Flanagan, R., and Nilsson, E. D.: Primary submicron marine aerosol dominated by insoluble organic colloids and aggregates, Geophysical Research Letters, 35, 2008.

Gard, E. E., Kleeman, M. J., Gross, D. S., Hughes, L. S., Allen, J. O., Morrical, B. D., Fergenson, D. P., Dienes, T., Galli, M. E., Johnson, R. J., Cass, G. R., and Prather, K. A.: Direct observation of heterogeneous chemistry in the atmosphere, Science, 279, 1184-1187, 10.1126/science.279.5354.1184, 1998.

Gaston, C. J., Furutani, H., Guazzotti, S. A., Coffee, K. R., Bates, T. S., Quinn, P. K., Aluwihare, L. I., Mitchell, B. G., and Prather, K. A.: Unique ocean-derived particles serve as a proxy for changes in ocean chemistry, Journal of Geophysical Research: Atmospheres, 116, 10.1029/2010jd015289, 2011.

Gaston, C. J., Pratt, K. A., Suski, K. J., May, N. W., Gill, T. E., and Prather, K. A.: Laboratory Studies of the Cloud Droplet Activation Properties and Corresponding Chemistry of Saline Playa Dust, Environmental Science & Technology, 51, 1348-1356, 10.1021/acs.est.6b04487, 2017.

Gaston, C. J., Cahill, J. F., Collins, D. B., Suski, K. J., Ge, J. Y., Barkley, A. E., and Prather, K. A.: The Cloud Nucleating Properties and Mixing State of Marine Aerosols Sampled along the Southern California Coast, Atmosphere, 9, 52, 2018.

Gysel, M., Crosier, J., Topping, D. O., Whitehead, J. D., Bower, K. N., Cubison, M. J., Williams, P. I., Flynn, M. J., McFiggans, G. B., and Coe, H.: Closure study between chemical composition and hygroscopic growth of aerosol particles during TORCH2, Atmospheric Chemistry and Physics, 7, 6131-6144, 2007.

Hatch, L. E., Pratt, K. A., Huffman, J. A., Jimenez, J. L., and Prather, K. A.: Impacts of Aerosol Aging on Laser Desorption/Ionization in Single-Particle Mass Spectrometers, Aerosol Science and Technology, 48, 1050-1058, 10.1080/02786826.2014.955907, 2014.

Healy, R. M., Evans, G. J., Murphy, M., Juranyi, Z., Tritscher, T., Laborde, M., Weingartner, E., Gysel, M., Poulain, L., Kamilli, K. A., Wiedensohler, A., O'Connor, I. P., McGillicuddy, E., Sodeau, J. R., and Wenger, J. C.: Predicting hygroscopic growth using single particle chemical composition estimates, Journal of Geophysical Research-Atmospheres, 119, 9567-9577, 10.1002/2014jd021888, 2014.

Herich, H., Kammermann, L., Gysel, M., Weingartner, E., Baltensperger, U., Lohmann, U., and Cziczo, D. J.: In situ determination of atmospheric aerosol composition as a function of hygroscopic growth, Journal of Geophysical Research-Atmospheres, 113, D16213, 10.1029/2008jd009954, 2008.

Herich, H., Kammermann, L., Friedman, B., Gross, D. S., Weingartner, E., Lohmann, U., Spichtinger, P., Gysel, M., Baltensperger, U., and Cziczo, D. J.: Subarctic atmospheric aerosol composition: 2. Hygroscopic growth properties, Journal of Geophysical Research-Atmospheres, 114, D13204, 10.1029/2008jd011574, 2009.

Hu, D., Qiao, L., Chen, J., Ye, X., Yang, X., Cheng, T., and Fang, W.: Hygroscopicity of Inorganic Aerosols: Size and Relative Humidity Effects on the Growth Factor, Aerosol and Air Quality Research, 10, 255-264, 10.4209/aaqr.2009.12.0076, 2010.

Huang, Y., Chen, H., Wang, L., Yang, X., and Chen, J.: Single particle analysis of amines in ambient aerosol in Shanghai, Environmental Chemistry, 9, 202-210, 10.1071/en11145, 2012.

Koehler, K. A., Kreidenweis, S. M., DeMott, P. J., Petters, M. D., Prenni, A. J., and Carrico, C. M.: Hygroscopicity and cloud droplet activation of mineral dust aerosol, Geophysical Research Letters, 36, L08805, 10.1029/2009gl037348, 2009.

Laborde, M., Crippa, M., Tritscher, T., Juranyi, Z., Decarlo, P. F., Temime-Roussel, B., Marchand, N., Eckhardt, S., Stohl, A., Baltensperger, U., Prevot, A. S. H., Weingartner, E., and Gysel, M.: Black carbon physical properties and mixing state in the European megacity Paris, Atmospheric Chemistry and Physics, 13, 5831-5856, 10.5194/acp-13-5831-2013, 2013.

Liu, H. J., Zhao, C. S., Nekat, B., Ma, N., Wiedensohler, A., van Pinxteren, D., Spindler, G., Muller, K., and Herrmann, H.: Aerosol hygroscopicity derived from size-segregated chemical composition and its parameterization in the North China Plain, Atmospheric Chemistry and Physics, 14, 2525-2539, 10.5194/acp-14-2525-2014, 2014.

Liu, P. F., Zhao, C. S., Gobel, T., Hallbauer, E., Nowak, A., Ran, L., Xu, W. Y., Deng, Z. Z., Ma, N., Mildenberger, K., Henning, S., Stratmann, F., and Wiedensohler, A.: Hygroscopic properties of aerosol particles at high relative humidity and their diurnal variations in the North China Plain, Atmospheric Chemistry and Physics, 11, 3479-3494, 10.5194/acp-11-3479-2011, 2011.

Liu, X. G., Zhang, Y. H., Cheng, Y. F., Hu, M., and Han, T. T.: Aerosol hygroscopicity and its impact on atmospheric visibility and radiative forcing in Guangzhou during the 2006 PRIDE-PRD campaign, Atmospheric Environment, 60, 59-67, 10.1016/j.atmosenv.2012.06.016, 2012.

Lohmann, U., and Feichter, J.: Global indirect aerosol effects: a review, Atmospheric Chemistry and Physics, 5, 715-737, 2005.

Petters, M. D., and Kreidenweis, S. M.: A single parameter representation of hygroscopic growth and cloud condensation nucleus activity, Atmospheric Chemistry and Physics, 7, 1961-1971, 2007.

Prather, K. A., Bertram, T. H., Grassian, V. H., Deane, G. B., Stokes, M. D., DeMott, P. J., Aluwihare, L. I., Palenik, B. P., Azam, F., Seinfeld, J. H., Moffet, R. C., Molina, M. J., Cappa, C. D., Geiger, F. M., Roberts, G. C., Russell, L. M., Ault, A. P., Baltrusaitis, J., Collins, D. B., Corrigan, C. E., Cuadra-Rodriguez, L. A., Ebben, C. J., Forestieri, S. D., Guasco, T. L., Hersey, S. P., Kim, M. J., Lambert, W. F., Modini, R. L., Mui, W., Pedler, B. E., Ruppel, M. J., Ryder, O. S., Schoepp, N. G., Sullivan, R. C., and Zhao, D.: Bringing the ocean into the laboratory to probe the chemical complexity of sea spray aerosol, Proceedings of the National Academy of Sciences, 201300262, 10.1073/pnas.1300262110, 2013.

Pratt, K. A., Hatch, L. E., and Prather, K. A.: Seasonal Volatility Dependence of Ambient Particle Phase Amines, Environmental Science & Technology, 43, 5276-5281, 10.1021/es803189n, 2009.

Pratt, K. A., and Prather, K. A.: Real-Time, Single-Particle Volatility, Size, and Chemical Composition Measurements of Aged Urban Aerosols, Environmental Science & Technology, 43, 8276-8282, 10.1021/es902002t, 2009.

Qin, X. Y., Pratt, K. A., Shields, L. G., Toner, S. M., and Prather, K. A.: Seasonal comparisons of single-particle chemical mixing state in Riverside, CA, Atmospheric Environment, 59, 587-596, 10.1016/j.atmosenv.2012.05.032, 2012.

Qiu, C., and Zhang, R. Y.: Multiphase chemistry of atmospheric amines, Physical Chemistry Chemical Physics, 15, 5738-5752, 10.1039/c3cp43446j, 2013.

Qu, W. J., Wang, J., Zhang, X. Y., Wang, D., and Sheng, L. F.: Influence of relative humidity on aerosol composition: Impacts on light extinction and visibility impairment at two sites in coastal area of China, Atmospheric Research, 153, 500-511, 10.1016/j.atmosres.2014.10.009, 2015.

Randles, C. A., Russell, L. M., and Ramaswamy, V.: Hygroscopic and optical properties of organic sea salt aerosol and consequences for climate forcing, Geophysical Research Letters, 31, 10.1029/2004gl020628, 2004.

Rehbein, P. J. G., Jeong, C.-H., McGuire, M. L., and Evans, G. J.: Strategies to Enhance the Interpretation of Single-Particle Ambient Aerosol Data, Aerosol Science and Technology, 46, 584-595, 10.1080/02786826.2011.650334, 2012.

Rissler, J., Vestin, A., Swietlicki, E., Fisch, G., Zhou, J., Artaxo, P., and Andreae, M. O.: Size distribution and hygroscopic properties of aerosol particles from dry-season biomass burning in Amazonia, Atmospheric Chemistry and Physics, 6, 471-491, 2006.

Shi, Y., Ge, M., and Wang, W.: Hygroscopicity of internally mixed aerosol particles containing benzoic acid and inorganic salts, Atmospheric Environment, 60, 9-17, 2012.

Silva, P. J., Liu, D. Y., Noble, C. A., and Prather, K. A.: Size and chemical characterization of individual particles resulting from biomass burning of local Southern California species, Environmental Science & Technology, 33, 3068-3076, 10.1021/es980544p, 1999.

Silva, P. J.: Source profiling and apportionment of airborne particles: A new approach using aerosol time-of-flight mass spectrometry, Ph.D., University of California, Riverside, United States -- California, 428-428 p. pp., 2000.

Sjogren, S., Gysel, M., Weingartner, E., Alfarra, M. R., Duplissy, J., Cozic, J., Crosier, J., Coe, H., and Baltensperger, U.: Hygroscopicity of the submicrometer aerosol at the high-alpine site Jungfraujoch, 3580 m a.s.l., Switzerland, Atmospheric Chemistry and Physics, 8, 5715-5729, 2008.

Song, X. H., Hopke, P. K., Fergenson, D. P., and Prather, K. A.: Classification of single particles analyzed by ATOFMS using an artificial neural network, ART-2A, Analytical Chemistry, 71, 860-865, 10.1021/ac9809682, 1999.

Spencer, M. T., Shields, L. G., Sodeman, D. A., Toner, S. M., and Prather, K. A.: Comparison of oil and fuel particle chemical signatures with particle emissions from heavy and light duty vehicles, Atmospheric Environment, 40, 5224-5235, 10.1016/j.atmosenv.2006.04.011, 2006.

Su, Y. X., Sipin, M. F., Furutani, H., and Prather, K. A.: Development and characterization of an aerosol time-of-flight mass spectrometer with increased detection efficiency, Analytical Chemistry, 76, 712-719, 10.1021/ac034797z, 2004.

Sullivan, R. C., Guazzotti, S. A., Sodeman, D. A., and Prather, K. A.: Direct observations of the atmospheric processing of Asian mineral dust, Atmospheric Chemistry and Physics, 7, 1213-1236, 2007.

Swietlicki, E., Hansson, H. C., Hameri, K., Svenningsson, B., Massling, A., McFiggans, G., McMurry, P. H., Petaja, T., Tunved, P., Gysel, M., Topping, D., Weingartner, E., Baltensperger, U., Rissler, J., Wiedensohler, A., and Kulmala, M.: Hygroscopic properties of submicrometer atmospheric aerosol particles measured with H-TDMA instruments in various environments - a review, Tellus Series B-Chemical and Physical Meteorology, 60, 432-469, 10.1111/j.1600-0889.2008.00350.x, 2008.

Toner, S. M., Shields, L. G., Sodeman, D. A., and Prather, K. A.: Using mass spectral source signatures to apportion exhaust particles from gasoline and diesel powered vehicles in a freeway study using UF-ATOFMS, Atmospheric Environment, 42, 568-581, 10.1016/j.atmosenv.2007.08.005, 2008.

Varutbangkul, V., Brechtel, F. J., Bahreini, R., Ng, N. L., Keywood, M. D., Kroll, J. H., Flagan, R. C., Seinfeld, J. H., Lee, A., and Goldstein, A. H.: Hygroscopicity of secondary organic aerosols formed by oxidation of cycloalkenes, monoterpenes, sesquiterpenes, and related compounds, Atmospheric Chemistry and Physics, 6, 2367-2388, 2006.

Wang, X. N., Ye, X. N., Chen, H., Chen, J. M., Yang, X., and Gross, D. S.: Online hygroscopicity and chemical measurement of urban aerosol in Shanghai, China, Atmospheric Environment, 95, 318-326, 10.1016/j.atmosenv.2014.06.051, 2014.

Weingartner, E., Burtscher, H., and Baltensperger, U.: Hygroscopic properties of carbon and diesel soot particles, Atmospheric Environment, 31, 2311-2327, 1997.

Ye, X., Tang, C., Yin, Z., Chen, J., Ma, Z., Kong, L., Yang, X., Gao, W., and Geng, F.: Hygroscopic growth of urban aerosol particles during the 2009 Mirage-Shanghai Campaign, Atmospheric Environment, 64, 263-269, 2013.

Ye, X. N., Chen, T. Y., Hu, D. W., Yang, X., Chen, J. M., Zhang, R. Y., Khakuziv, A. F., and Wang, L.: A Multifunctional HTDMA System with a Robust Temperature Control, Advances in Atmospheric Sciences, 26, 1235-1240, 10.1007/s00376-009-8134-3, 2009.

Ye, X. N., Ma, Z., Hu, D. W., Yang, X., and Chen, J. M.: Size-resolved hygroscopicity of submicrometer urban aerosols in Shanghai during wintertime, Atmospheric Research, 99, 353-364, 10.1016/j.atmosres.2010.11.008, 2011.

Zauscher, M. D., Wang, Y., Moore, M. J. K., Gaston, C. J., and Prather, K. A.: Air Quality Impact and Physicochemical Aging of Biomass Burning Aerosols during the 2007 San Diego Wildfires, Environmental Science & Technology, 47, 7633-7643, 10.1021/es4004137, 2013.

Zelenyuk, A., Imre, D., Han, J. H., and Oatis, S.: Simultaneous measurements of individual ambient particle size, composition, effective density, and hygroscopicity, Analytical Chemistry, 80, 1401-1407, 10.1021/ac701723v, 2008.

Zhang, G., Bi, X., Chan, L. Y., Li, L., Wang, X., Feng, J., Sheng, G., Fu, J., Li, M., and Zhou, Z.: Enhanced trimethylamine-containing particles during fog events detected by single particle aerosol mass spectrometry in urban Guangzhou, China, Atmospheric Environment, 55, 121-126, 10.1016/j.atmosenv.2012.03.038, 2012.

Zhang, Q., Jimenez, J. L., Canagaratna, M. R., Allan, J. D., Coe, H., Ulbrich, I., Alfarra, M. R., Takami, A., Middlebrook, A. M., Sun, Y. L., Dzepina, K., Dunlea, E., Docherty, K., DeCarlo, P. F., Salcedo, D., Onasch, T., Jayne, J. T., Miyoshi, T., Shimono, A., Hatakeyama, S., Takegawa, N., Kondo, Y., Schneider, J., Drewnick, F., Borrmann, S., Weimer, S., Demerjian, K., Williams, P., Bower, K., Bahreini, R., Cottrell, L., Griffin, R. J., Rautiainen, J., Sun, J. Y., Zhang, Y. M., and Worsnop, D. R.: Ubiquity and dominance of oxygenated species in organic aerosols in anthropogenically-influenced Northern Hemisphere midlatitudes, Geophysical Research Letters, 34, L13801, 10.1029/2007gl029979, 2007.

ACKNOWLEDGMENT

This work was supported by the National Natural Science Foundation of China (Nos. 91544224, 21906024, 41775150, 41827804), Shanghai Natural Science Foundation (No. 19ZR1404000) and the Program for Guangdong Introducing Innovative and Entrepreneurial Teams (2017ZT07Z479). We acknowledge the Shanghai Environmental Monitoring Center for providing ambient air quality data.

TABLES

Table 1. Statistics of the DRH, GF, sampling duration and the number of chemically analyzed particles by ATOFMS (D_{dry} = 250 nm, RH = 85%).

D_{RH} (nm)	225	250	275	300	325	350	375	400	425
Growth Factor	0.9	1.0	1.1	1.2	1.3	1.4	1.5	1.6	1.7
Duration (hours)	42	67	11	20	8	11	34	20	11
Number of particle spectra	742	1665	709	1401	2330	4469	6399	723	262

Table 2. Statistics on particle number contributions of ATOFMS particle types to different GF modes. The statistics are the average contributions and variation ranges (in brackets) based on temporal data in daily resolution.

Contribution (%)	**NH (GF <1.1)**	**LH (GF 1.1-1.3)**	**MH (GF 1.3-1.5)**	**SS (GF >1.5)**
Fresh EC	14 (7-17)	2 (1-4)	0 (0-3)	0 (0-1)
Cooking	3 (0-7)	1 (0-3)	0 (0-0)	0 (0-0)
Biomass	18 (7-35)	9 (2-17)	0 (0-1)	0 (0-0)
HMOC	40 (30-68)	8 (2-15)	0 (0-1)	0 (0-0)
Ammonium/OC	11 (3-21)	32 (20-45)	2 (1-5)	0 (0-0)
Aged EC	2 (1-5)	12 (5-20)	47 (15-72)	13 (1-42)
Dust/ash	3 (1-6)	13 (9-22)	27 (13-53)	26 (4-44)
Amine-rich	3 (1-5)	12 (2-41)	13 (4-39)	11 (1-44)
Sea salt	0 (0-1)	0 (0-1)	1 (0-4)	40 (7-78)

FIGURES

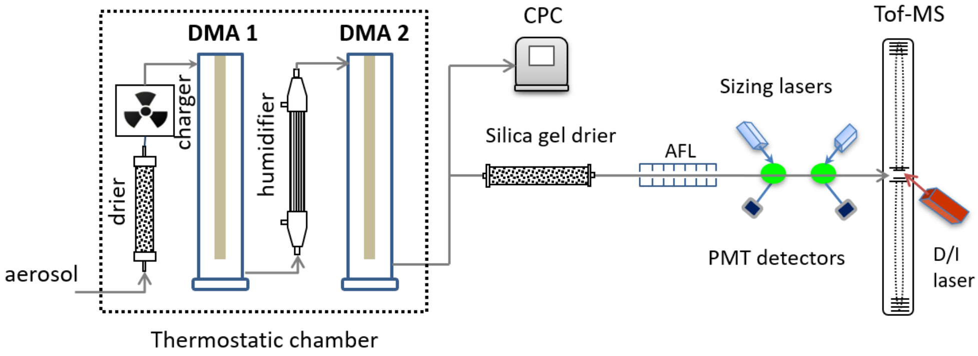

Figure 1. The schematic of HTDMA-ATOFMS characterization setup showing the major parts of HTDMA (left), ATOFMS (right). The humidifier in HTDMA was maintained at 85% RH.

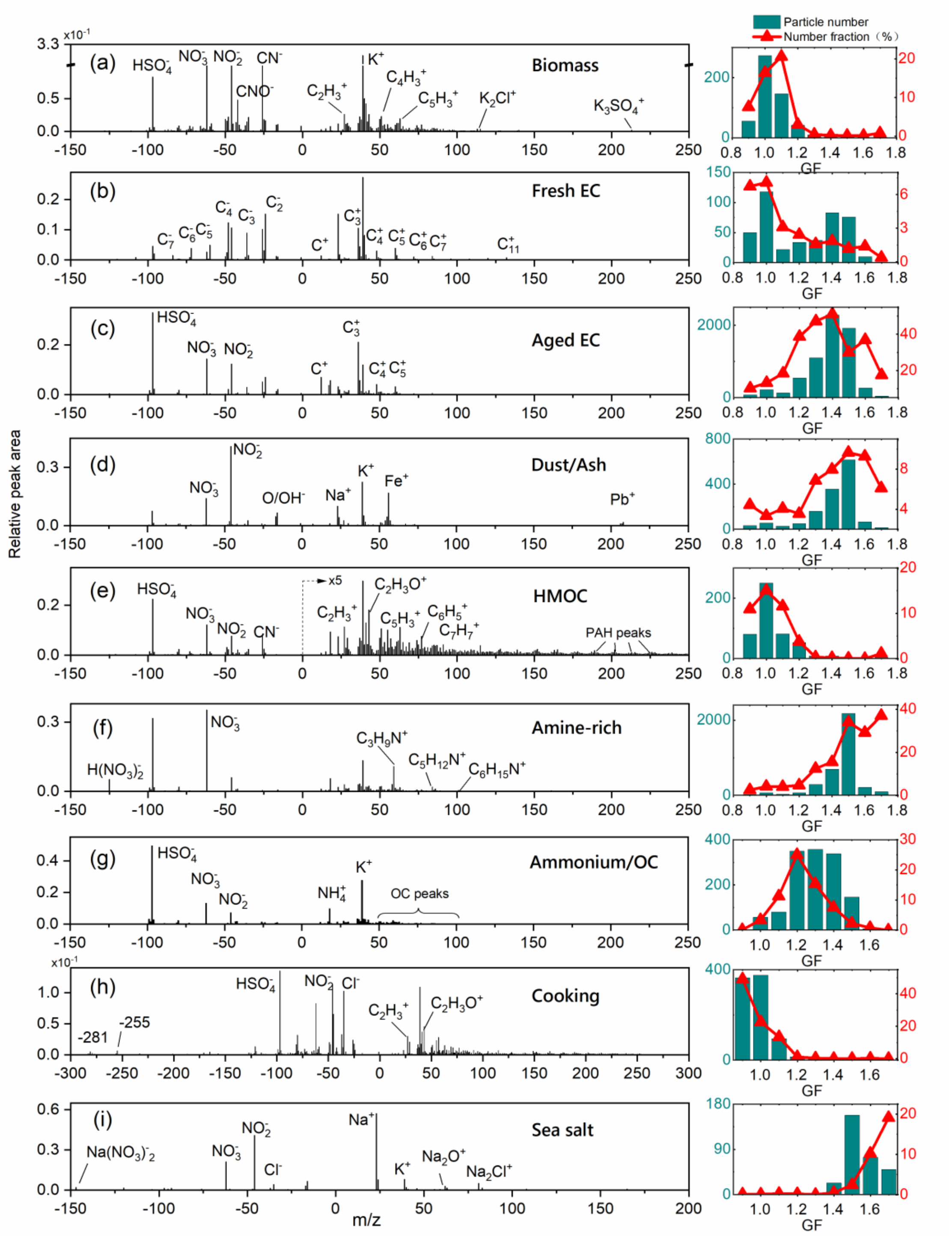

Figure 2. (Left panel) Averaged particle mass spectra of the major particle types detected in HTDMA-ATOFMS characterization. Peaks of significance were labelled. Right panels show the particle numbers of each type (left-axis) and their relative number fractions in total particles (right-axis) as a function of GF.

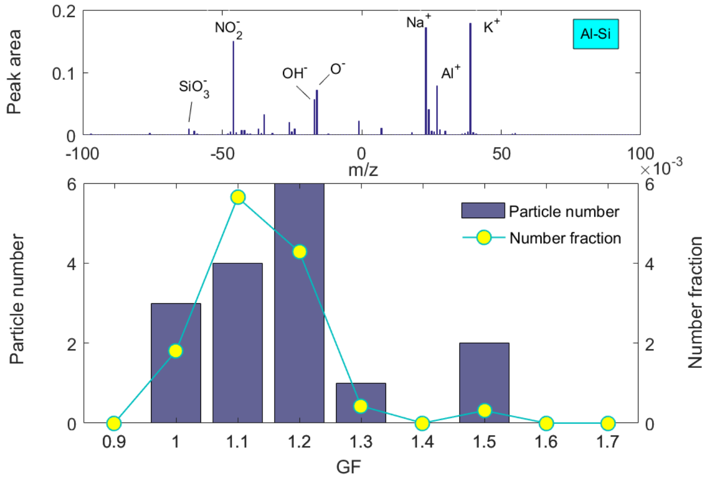

Figure 3. Average mass spectra and hygroscopicity distribution of Al-Si particles.

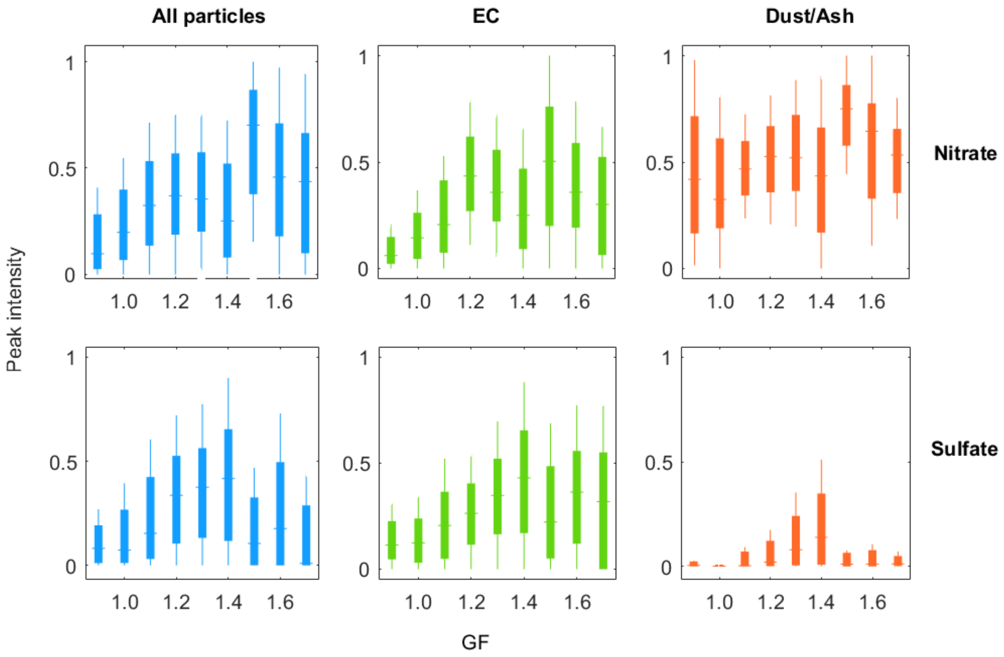

Figure 4. Statistics of nitrate and sulfate peak intensities (minimum, 25th percentile, median, 75th percentile, maximum) with GF in HTDMA-ATOFMS experiment. The intensity statistics were calculated for All particles, EC particles and Dust/Ash particles separately.

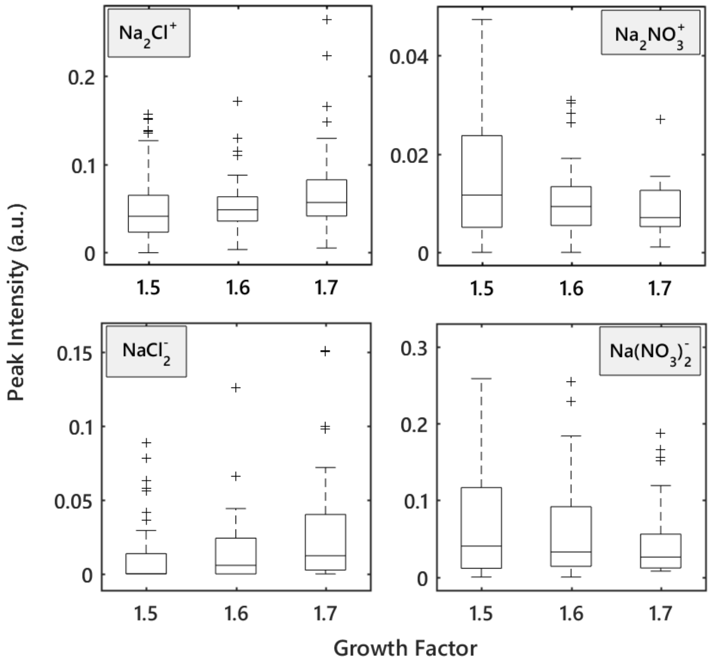

Figure 5. Statistics of peak intensities in sea salt particle mass spectra in GF 1.5-1.7 range. The statistics include minimum, 25th percentile, median, 75th percentile, maximum and outliers for each GF bin.

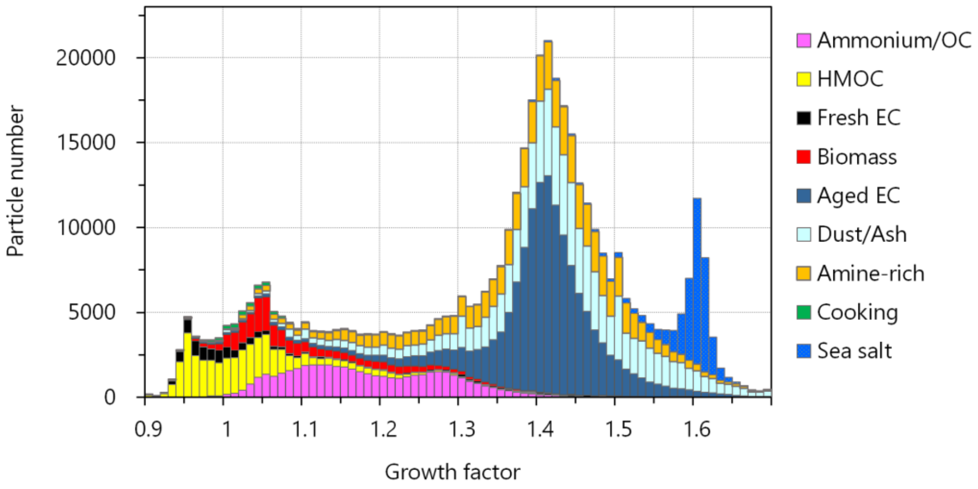

Figure 6. Particle number distribution of different particle types as a function of estimated GF during Sep-12 to Sep-28, 2012.

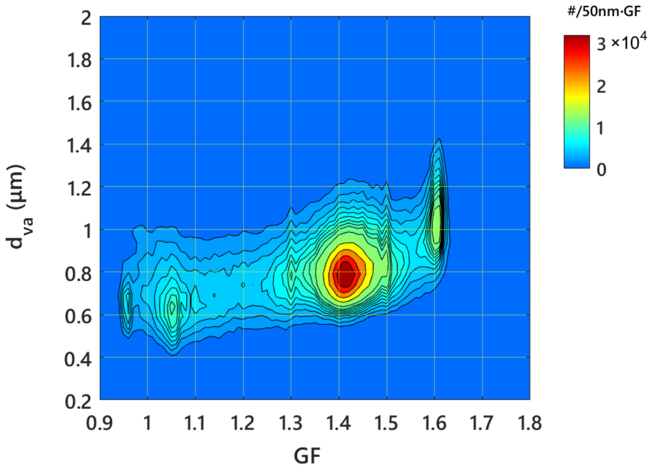

Figure 7. The distribution of ATOFMS particles as a bivariate function of estimated GF and aerodynamic diameter.

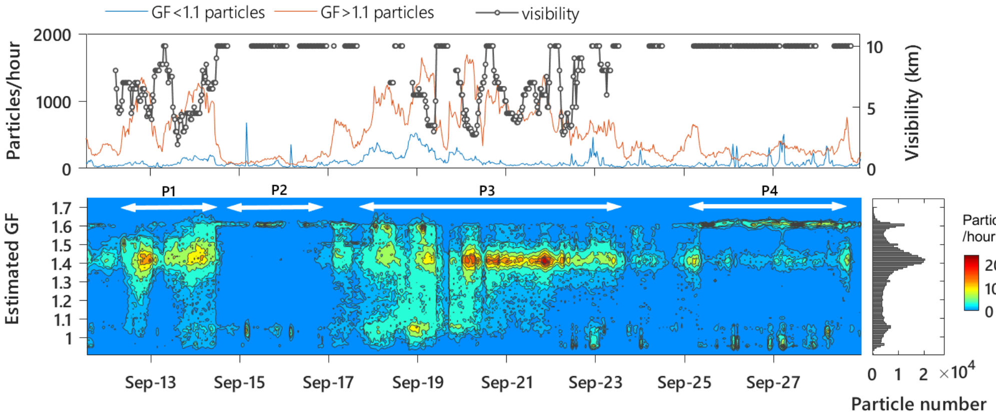

Figure 8. Temporal variations of atmospheric visibility and number concentrations of nearly-hydrophobic (estimated GF < 1.1) and hygroscopic (GF >1.1) particles (Upper). The lower panel show the temporal variation of estimated GF from Sep-12 to Sep-28, 2012. In the lower-right panel is the particle number distribution with GF during the period.

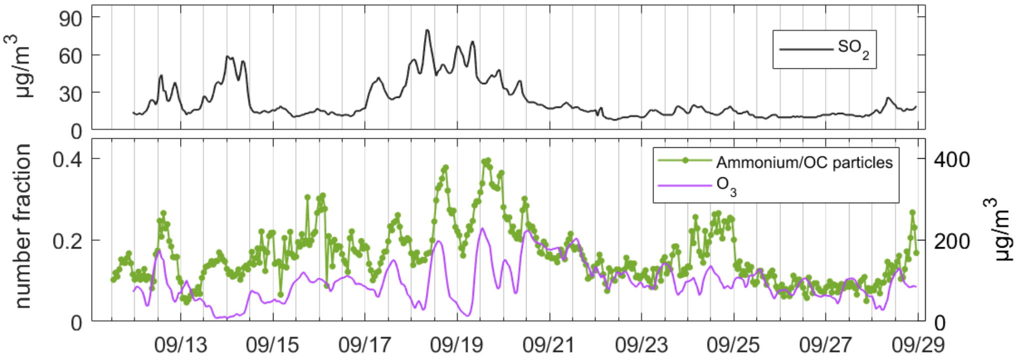

Figure 9. Temporal traces of Ammonium/OC relative number concentrations, ambient O_3 and SO_2 concentrations during Sep-12 to Sep-28, 2012

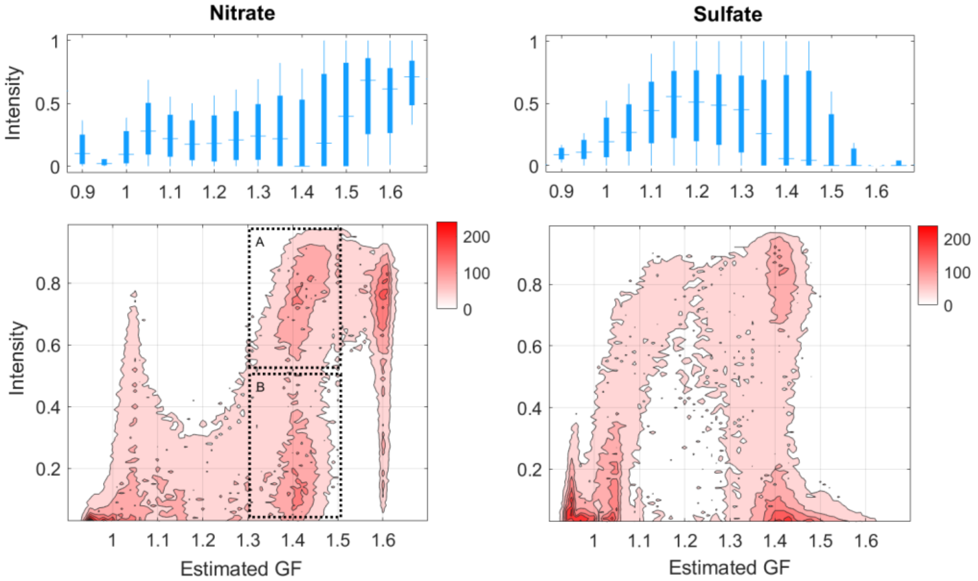

Figure 10. Statistics (minimum, 25th percentile, median, 75th percentile, maximum) on the nitrate and sulfate peak intensities of ambient particles at different GFs (upper). The lower panels show particle distributions as a bivariate function of estimated GF and peak intensities of nitrate and sulfate.

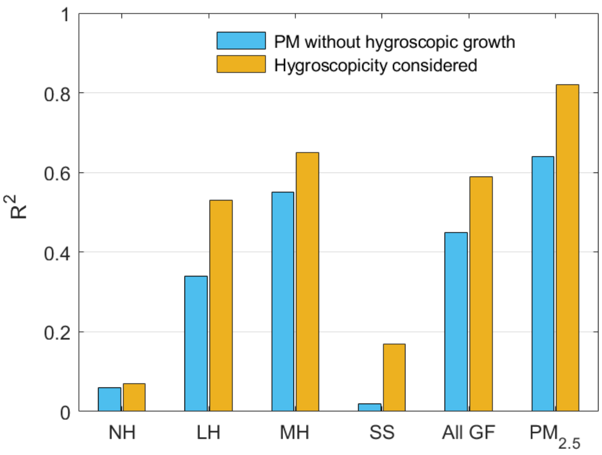

Figure 11. The R-squares between visibility and PM volume concentrations with and without considering particle hygroscopicity